



# Synthesis of Pd-Cu/TPPCu electrocatalyst for direct ethanol fuel cell applications

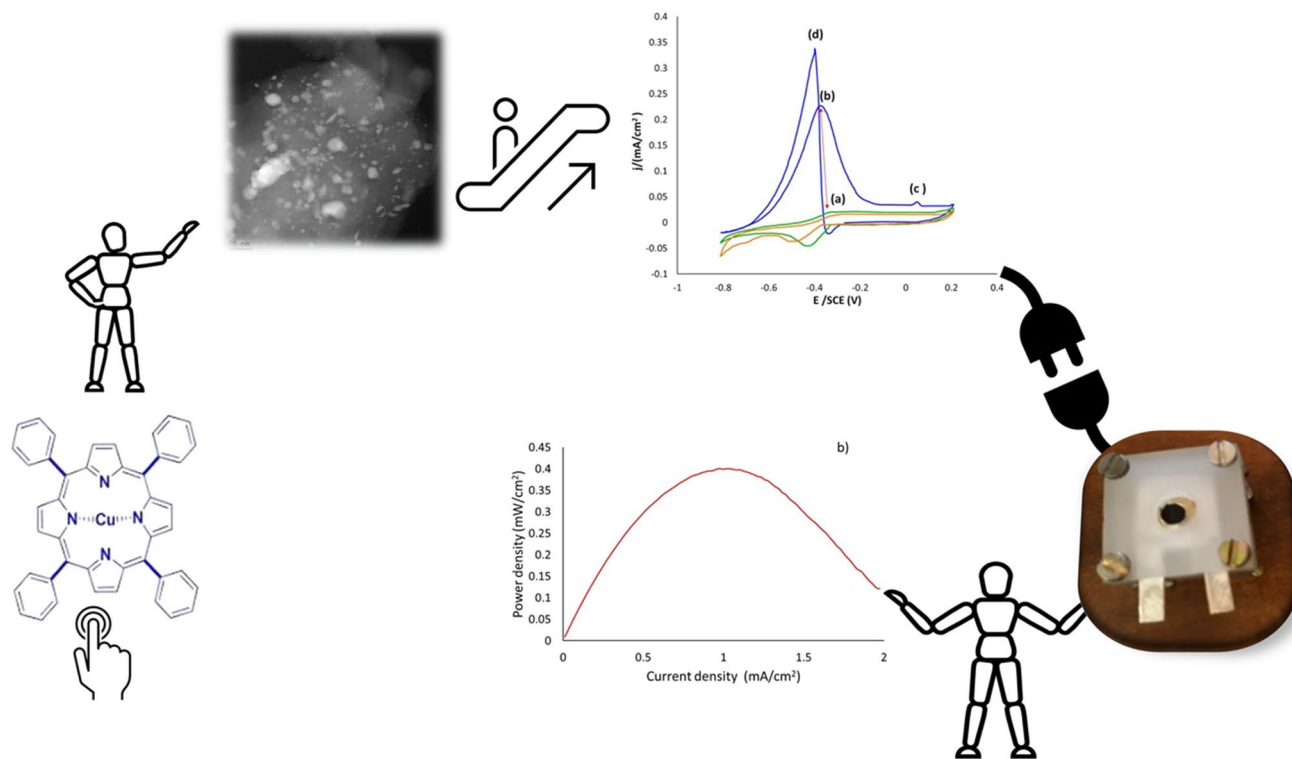
S. Irazoque<sup>1,2</sup> · A. López-Suárez<sup>3</sup> · C. K. Zagal-Padilla<sup>1,2</sup> · S. A. Gamboa<sup>1</sup>

Received: 28 June 2023 / Accepted: 1 October 2023 / Published online: 3 November 2023  
© The Author(s) 2023

## Abstract

In this study, the electro-oxidation reaction of ethanol over Pd–Cu supported on Cu porphyrin (TPPCu) was investigated. The catalyst was synthesized using the microwave-assisted polyol method and physicochemically characterized by XRD, XPS, SEM, EDS, TEM, EDAX, UV–Vis, FTIR, and RBS. A Cu-enriched catalyst with Cu<sub>3</sub>Pd, Pd,Cu, and TPPCu phases was identified using XRD and XPS. However, according to the RBS results, the catalytic surface was enriched with Pd, indicating that the interaction between TPPCu and Pd–Cu allowed the presence of Pd on the surface, thus enhancing the catalytic response of the material. This synthesis prevented the deprotonation of porphyrin on the electrocatalyst, as confirmed by XPS analysis. Electrochemical studies based on cyclic voltammetry and electrochemical impedance spectroscopy were used to investigate the response of the catalyst to variations in the scan rate and increasing ethanol concentration. The electrochemical response of PdCu/TPPCu improved with an increasing number of cycles, indicating improved mass transport, thus improving its electrochemical response and tolerance to CO contamination. This catalyst exhibited a high electroactive surface area of 49.4 m<sup>2</sup>/g, which could be related to the presence of TPPCu as a support. The behavior of the catalyst on the anode of a fuel cell fed with ethanol, bioethanol, and bioethanol residues was evaluated.

## Graphical Abstract



**Keywords** Electro-oxidation · Metalloporphyrin · Alkaline media · Bioethanol · Fuel cell

## 1 Introduction

Fuel cells are electrochemical devices that convert chemical energy into electricity [1]. Ethanol is a high-energy fuel with low toxicity in humans. Owing to their compact design and expected long-life performance, direct ethanol fuel cells in alkaline media are promising devices for next-generation electric vehicles, mobile phones, and 5G communication systems [2]. Alcohol can also be produced using fossil fuels and biomass fermentation processes [3, 4].

There are some problems related to the low-energy conversion efficiency, poisoning of electrocatalysts, high-activation energy required to initiate the ethanol electro-oxidation reaction (EOR), high overpotential to activate the ethanol electro-oxidation reaction, and unstable conducting supports for electrocatalysts operating in alkaline media [5–7].

The search for suitable catalysts and supports remains a challenge in materials science. Extensive research has been conducted to address this issue. The use of bimetallic materials has opened the possibility of obtaining electrocatalysts with sufficient lifetime to perform the ethanol electro-oxidation reaction in alkaline media. Historically, compounds based on Pt–Sn, Pt–Ru, and Pt–Ni have shown

the best electrocatalytic properties for the EOR. However, the adsorption of CO-based intermediate species and its influence on the depletion of electrocatalytic activity have limited the development of commercial ethanol fuel cells [8, 9]. To solve this problem, Pd-based electrocatalysts have been considered as feasible materials for promoting the development of commercial fuel cells. Pd exhibits good electrocatalytic properties for the EOR in alkaline fuel cells. It exhibits good resistance to poisoning effects owing to CO adsorption. It is easy to obtain alloys and composites with other metals, which improves the operating life of fuel cells [10–12].

It has been demonstrated that the use of a second metal in a Pd-based composite modifies the d-band center, which improves the catalytic activity for EOR and tolerance to CO species [13]. It is also possible to increase the activity and selectivity of the reaction by controlling the composition and morphology of electrocatalysts [14]. Some examples of Pd-based electrocatalysts include Pd/C, Pd–Ru/C, AuAg, PdFeCo, Pd/Al–Mg–Ag, Pd–Ag, Pd–Au/, Pd–Ag/C, Pt–Rh/C, and PdNiBi/C, which exhibit high-catalytic activity, durability, and stability in alkaline media [15–20].

Similarly, Pd–Cu nanoparticles showed good electrocatalytic activity for the EOR. In this case, Cu increases

the tolerance to poisoning by intermediate species [21, 22]. Suitable support is crucial for the performance of electrocatalysts during EOR. Therefore, in this study, we propose the use of a Cu-coordinated metalloporphyrin (TPPCu) as a support material. TPPCu has been widely used because of its exceptional optoelectronic properties, which are beneficial for photosynthetic processes. TPPCu also exhibits hydrophilic properties [23–26] and can adsorb ethanol in the electrocatalytic layer to ensure electro-oxidation. In this study, a PdCu/TPPCu catalyst was synthesized by the microwave-assisted polyol method for application as the anode of an ethanol fuel cell. The results of physicochemical and electrochemical studies indicated that the catalyst support played an important role in the operation of the catalyst during anodic reactions. The electrocatalyst was evaluated in an alkaline direct ethanol fuel cell, where reagent-grade ethanol, bioethanol, and its waste were used to feed the electrochemical device.

## 2 Experimental methods

### 2.1 Synthesis of PdCu/TPPCu electrocatalyst

PdCu/TPPCu was synthesized by the microwave-assisted polyol method using 268 mg PdCl<sub>2</sub> (palladium(II) chloride, 99% purity, Fermont), 166.6 mg CuCl<sub>2</sub>·2H<sub>2</sub>O (copper(II) chloride dihydrate, 99.4% purity, Fermont), and 500 mg TPPCu (5, 10, 15, 20-tetraphenyl-21H,23H-porphine copper(II), 97% purity, Sigma-Aldrich).

The precursor salts were dissolved in 40 mL C<sub>2</sub>H<sub>6</sub>O<sub>2</sub> (98% purity, Fermont) under ultrasonication for 60 min. The solution was then transferred to a Synthos 3000 Anton Par (microwave synthesis platform). Synthesis was performed at 130 °C (600 W) for 30 min. The powder was introduced into a SOLBAT c-40 centrifuge for 15 min at 2500 rpm in a 1:1 solution of CH<sub>3</sub>CH<sub>2</sub>OH (99.9% purity, Fermont) and (CH<sub>3</sub>)<sub>2</sub>CO (99.7% purity, Fermont). The catalytic powder was dried at 50 °C for 2 h using a conventional magnetic heater.

### 2.2 Characterization of PdCu/TPPCu

Structural characterization was performed by X-ray diffraction (XRD) using a Rigaku diffractometer (model DMAX 2200) with an incident signal of monochromatic radiation (CuK $\alpha$ 1 line,  $\lambda = 1.54$  Å, copper filament). XPS characterization was performed on a Thermo Scientific K-alpha model with a monochromatic aluminum (Al k $\alpha$ ) X-ray source at 1486.6 eV energy, using a spot size of 400  $\mu$ m. For the survey-type scans, a pass energy of 200 eV and an energy step size of 1 eV were used. For the high-resolution scans,

values of 50 eV and 0.1 eV, respectively, were used. The experimental data were referenced to an adventitious carbon peak (C 1 s) at 284.6 eV. All spectra were fitted to this value. A Hitachi S-5500 FE-SEM microscope was used to investigate the morphology and chemical composition of the samples by scanning electron microscopy (SEM) and energy-dispersive X-ray spectroscopy (EDS). High-resolution transmission electron microscopy (HRTEM) images of PdCu/TPPCu were obtained using a JEOL TEM-2010 FEG electron microscope with 200 keV acceleration and 0.19 nm spot resolution. The material was deposited on a Cu grid for microscopic analysis. Absorption spectra were obtained using a V-630 UV–Vis spectrophotometer in the wavelength range 350–700 nm. The chemical bonding structure of the materials was analyzed using a Perkin Elmer GX3 Fourier Transform Infrared (FTIR) spectrometer in the 4000–500 cm<sup>-1</sup> range. The elemental concentration was determined using Rutherford backscattering spectrometry (RBS) in a 3 MV tandem accelerator (NEC 9SDH-2 Pelletron) with a 3 MeV alpha particle beam of 1 mm diameter. The RBS spectra were simulated and analyzed using SIMNRA code version 6.04.

The catalytic ink for the working electrode was prepared in an ultrasonic bath for 20 min using 2 mg of PdCu/TPPCu, 5  $\mu$ L of liquid Nafion (liquid solution LQ-1105 1100EW at 5 wt.%), and 10  $\mu$ L of 2-propanol (99.9% purity, Fermont). Catalytic ink (5  $\mu$ L) was deposited on the glassy carbon surface (area of 0.071 cm<sup>2</sup>) of a rotating disk electrode and dried at room temperature.

Electrochemical characterization was performed in a three-electrode electrochemical cell using a saturated calomel electrode (SCE) as the reference potential, a platinum mesh as the counter electrode, and a working electrode. The electrolyte was prepared using 1 M KOH (34 mL) and CH<sub>3</sub>CH<sub>2</sub>OH (1 mL). The electrochemical measurements were performed at 25 °C using a Metrohm Autolab 302NFRA potentiostat/galvanostat.

PdCu/TPPCu (8 mg) was dissolved in 25  $\mu$ L liquid Nafion and 50  $\mu$ L C<sub>3</sub>H<sub>8</sub>O. The catalytic ink was deposited on a 1 cm<sup>2</sup> carbon cloth (anode). The same procedure was used to prepare the catalytic ink from commercial Pt/C. However, in this case, the catalytic ink was deposited on a 1 cm<sup>2</sup> Teflon-treated carbon cloth to obtain the cathode of the fuel cell.

The anion exchange membranes (AMI 7001S, 1 cm<sup>2</sup>) were activated in 30 mL of 1 M KOH at 85 °C for 24 h. The membranes were maintained in 35 mL deionized H<sub>2</sub>O at 30 °C for 30 min and stored at room temperature. The electrodes and membrane were pressed with a thermoplate at 150 °C and 100 kg cm<sup>2</sup> for 30 min to obtain the fuel cell assembly.

### 3 Results

#### 3.1 X-ray diffraction

Figure 1 shows the XRD pattern of TPPCu. Peaks were identified at 8.6°, 11.78°, 15.16°, 19.88°, 22.22°, and 25.44°, corresponding to the Miller indices (022), (121), (131), (221), (151), and (114), respectively. Cu<sub>3</sub>Pd phase peaks were identified at 32.35°, 42.31°, 49.69°, and 72.54°. The characteristic planes were (2014), (117), (0014), and (2014). The Pd phase peaks were located at 40.19°, 46.73°, 68.19°, 82.17°, and 86.69°, corresponding to the (111), (200), (220), (311), and (222) planes, respectively. Crystalline Cu peaks were observed at 43.29° and 50.43°, corresponding to the (111) and (200) planes, respectively. JCPDS cards Nos. 00-054-130, 07-0138, 46-1043, and 04-0836 were used to identify the crystalline phases of TPPCu, Cu<sub>3</sub>Pd, Pd, and Cu, respectively. Finally, these results showed that the synthesis promoted the formation of an alloyed phase of Pd–Cu (Cu<sub>3</sub>Pd), as well as separated particles of Pd, Cu, supported on TPPCu.

The mean particle size of the phases identified in PdCu/TPPCu was calculated using the Debye–Scherrer equation (Eq. 1).

$$D = \frac{k \cdot \lambda}{\beta \cdot \cos \theta} \quad (1)$$

where  $D$  is the average particle size (Å),  $K$  is the Scherrer constant (0.89),  $\lambda$  is the radiation wavelength (1.54 Å),  $\beta$  is the full width at half maximum (FWHM), and  $\theta$  is the diffraction angle (rad).

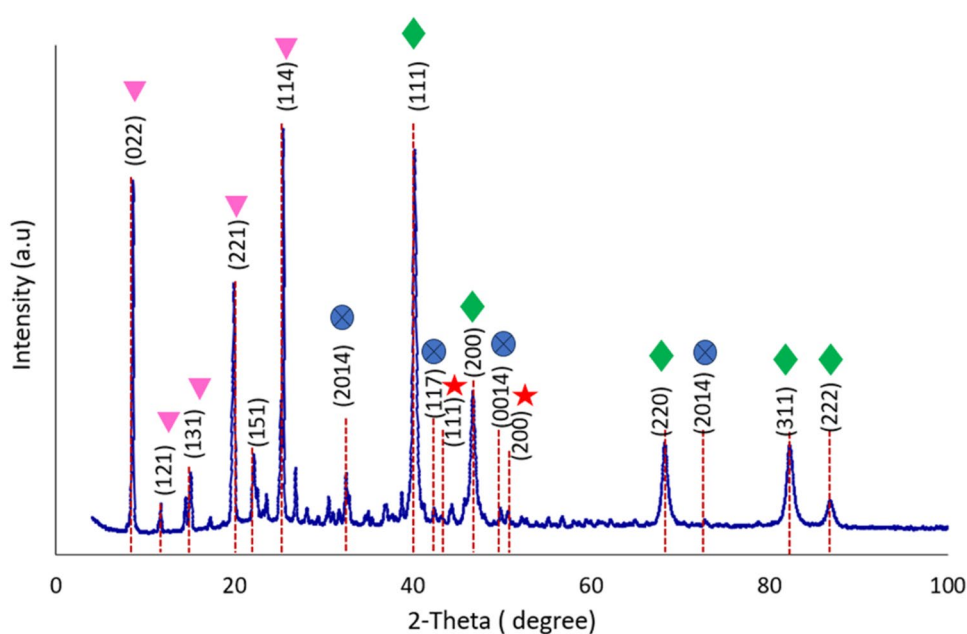
According to the calculations performed, the average particle size of TPPCu is 5.8348 Å. Copper coordinated to metalloporphyrin has an average particle size of 5.1163 Å. It was also observed that the Cu<sub>3</sub>Pd phase has an average particle size of 4.1510 Å, and for the Pd phase is 2.8154 Å. The above results suggest that copper metalloporphyrin, having a larger particle size, ensures the deposition of smaller electrocatalytic particles such as Cu<sub>3</sub>Pd and Pd.

#### 3.2 XPS analysis

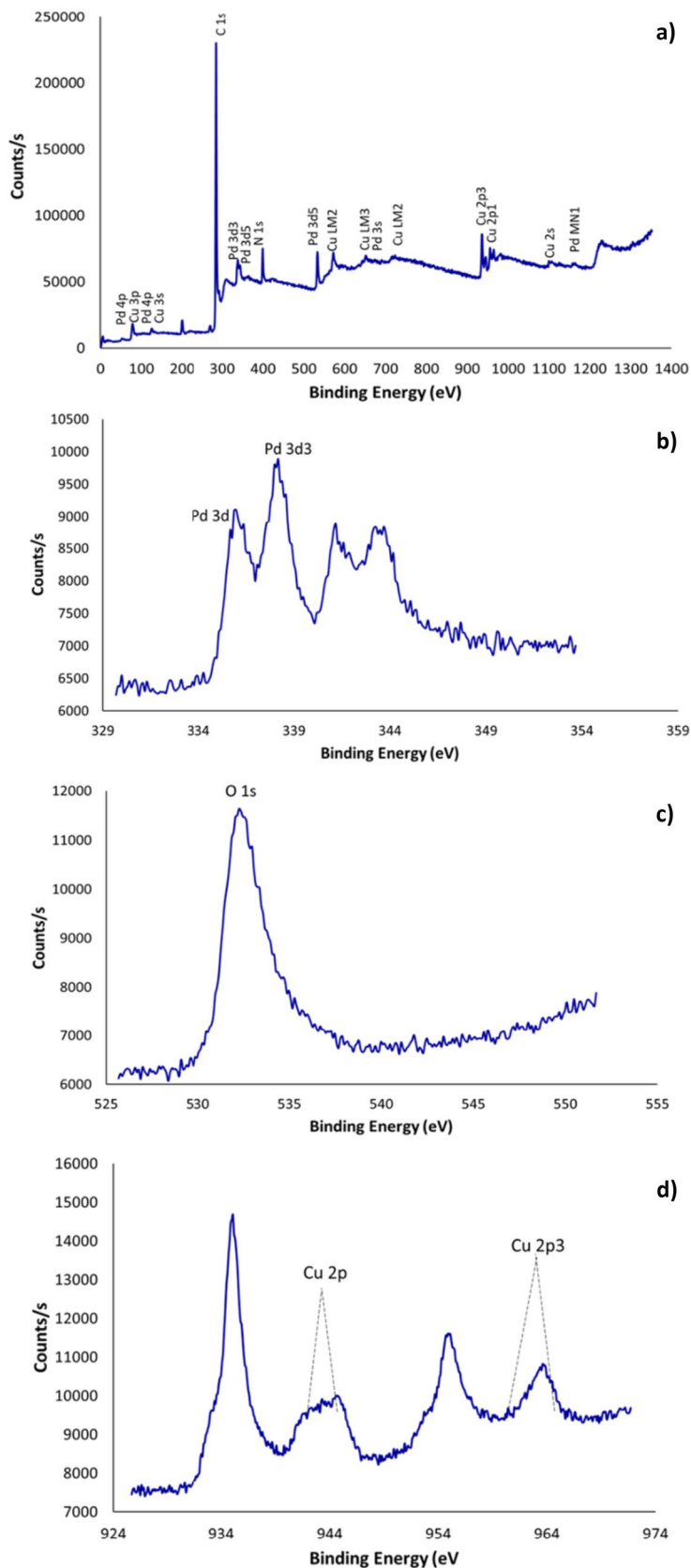
Figure 2 shows the XPS spectrum of the PdCu/TPPCu sample used to determine the composition and chemical state of the catalyst components. Figure 2a shows the presence of Pd and Cu. The elements are mainly shown: Pd 4p at 66.08 and 108.08 eV, Pd 3d<sub>3</sub> at 335.09 and 338.01 eV, Pd 3d<sub>5</sub> at 351.08 eV, Pd 3s at 532.08 eV, Pd 3s at 687.08 eV and Pd MN1 at 1177.08 eV. While Cu in its different energetic states was found at Cu 3p at 89.08 eV, Cu 3s at 138.08 eV, Cu LM2 at 585.08 eV, Cu LM2 at 731.08 eV, Cu 2p<sub>3</sub> at 945.08 eV, Cu 2P1 at 965.08 eV and Cu 2s at 117.08 eV. An overlapping peak at 332.48 eV is also observed, which is related to the presence of O 1s. A weak emission at 400.08 eV, corresponding to N 1s, was also found, indicating that in some cases, the metalloporphyrin rings were unable to coordinate with a Cu [27]. The weak N 1s signal indicates a minimal amount of deprotonated metalloporphyrin, suggesting that the organometallic molecule was not affected by the experimental synthesis conditions.

The best-defined phases were used as references. Twenty high-resolution scans were performed to compensate for the

**Fig. 1** XRD pattern of PdCu/TPPCu. Cu<sub>3</sub>Pd (◆), Pd (★), Cu (▼) y TPPCu



**Fig. 2** XPS spectra of PdCu/TPPCu. Survey spectrum (a) Elemental spectrum of Pd 3d3 (b). Elemental spectrum of O 1s (c). Elemental spectrum of Cu 2p (d)



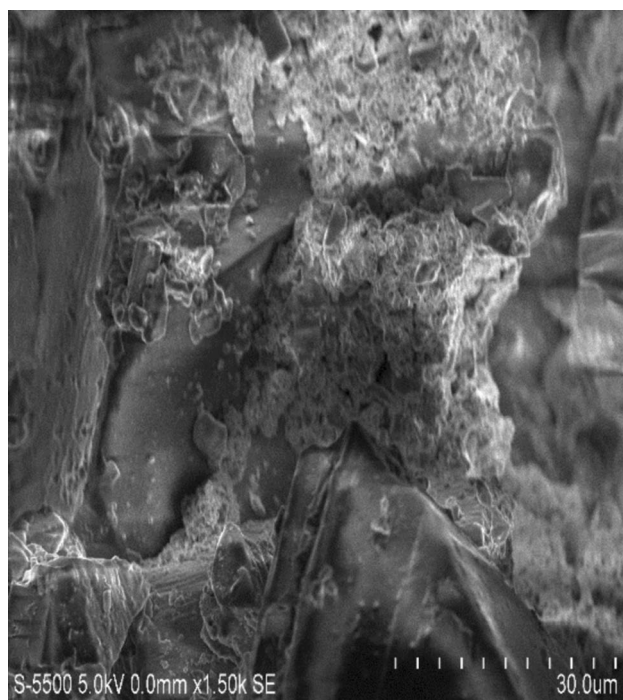


**Fig. 3** Micrograph of PdCu/TPPCu

low amount of the catalytic material in the sample. Figure 2b shows the high-resolution spectrum of Pd 3d, where it was possible to identify the presence of 2 oxidation states for Pd at 335.9 eV (which could be attributed to metallic Pd) and at 338.1 eV associated with a possible metal oxide, both with their respective doublets and a separation of 5.26 eV between the peaks.

Another 20 high-resolution scans were performed on the O 1s state to identify the possible origin of the oxide formation. Figure 2c shows the formation of an O 1s peak between 530 and 535 eV. This peak was superimposed on the Pd 3d peaks, indicating that it may be the precursor for the formation of the oxide observed at 338.1 eV.

Similarly, 20 high-resolution scans were performed for Cu 2p. Figure 2d shows the presence of satellites at about 943–945 eV and 962–965 eV, characteristic peaks of Cu(II) in the metalloporphyrin. Notably, the presence of Cu(II) in metalloporphyrins can lead to different behaviors [28] such as (i) the transfer of electron density from the metal surface to a metalloporphyrin complex, (ii) the formation of binding energy by the formation of Cu(I) complexes, and (iii) the presence of an oxidation state of the second Cu(I) ion [29].

The XPS study allowed us to identify in more detail the chemical species and oxidation states of the elements that comprise the phases present in the PdCu/TPPCu catalyst. Further research is required to identify the role of each species in electrochemical reactions, especially in complex reactions such as those associated with the oxidation of alcohols.

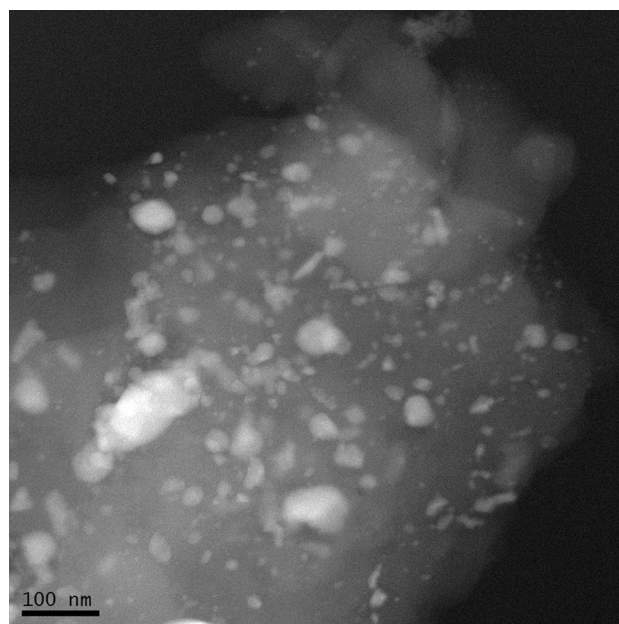


**Fig. 4** TEM image of PdCu/TPPCu. The diffuse shaded area corresponds to the TPPCu support. The bright particles correspond to the PdCu deposited on the TPPCu surface

### 3.3 Physicochemical characterization

Figure 3 shows a micrograph of Pd–Cu/TPPCu. The agglomerated filaments are associated with the formation of the Pd–Cu phase, as previously discussed using XRD. The observed 3D surface corresponded to TPPCu, because this metalloporphyrin usually synthesizes with a very large surface area, which is suitable as a support for PdCu [30]. This synthesis promoted the deposition of electrocatalytic particles on the surface of the TPPCu. The chemical composition of the sample was 80.85% C, 7.63% N, 4.31% Pd, and 7.21% Cu (as measured by EDS). The C and N contents were consistent with the organic composition of the TPP. The Pd/Cu ratio (0.59) indicated that Cu was more exposed to Pd on the surface of the electrocatalyst.

### 3.4 TEM analysis

Figure 4 shows the TEM image of PdCu/TPPCu. It was possible to observe the presence of the TPPCu support as a diffuse spot with a light background on which dispersed PdCu particles were deposited. The dark background in the image indicates the carbon support. It is observed that the TPPCu has a large surface area where the PdCu particles are located. It is possible that the dispersion of the catalytic particles on the support was a function of the active centers related to the coordination of the metalloporphyrin with its Cu center. This process, as well as the size of the synthesized PdCu particles, were influenced by the synthesis method. Clusters

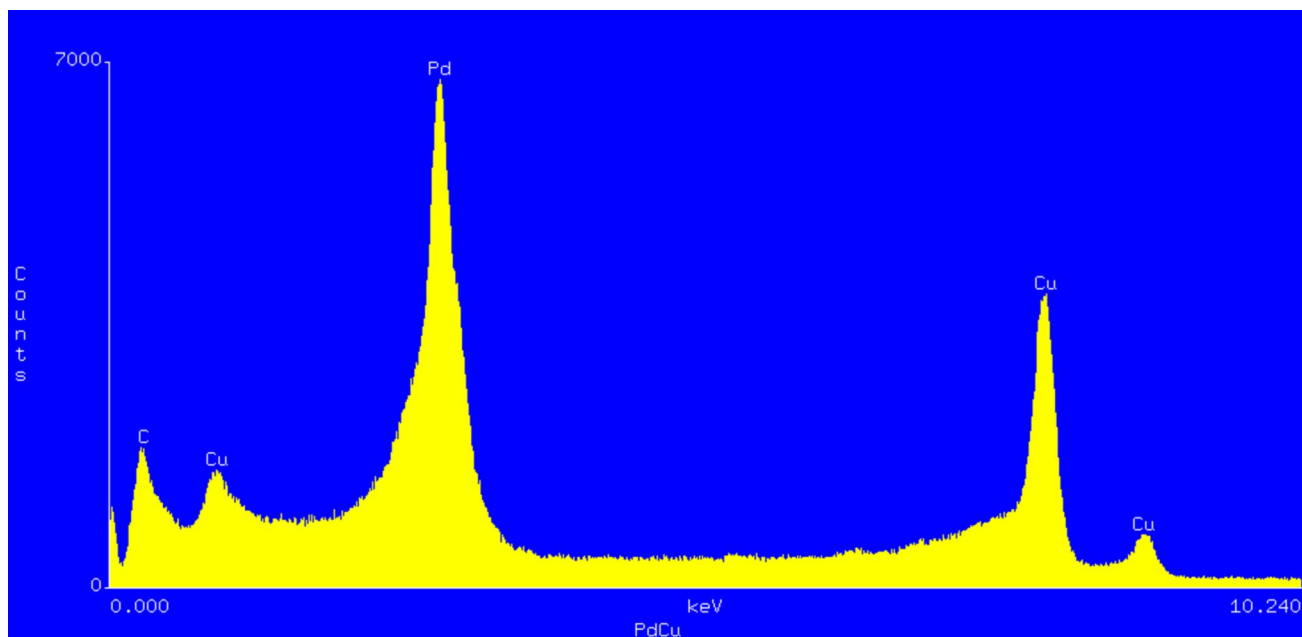


**Fig. 5** EDAX report of Pd Cu supported on TPPCu

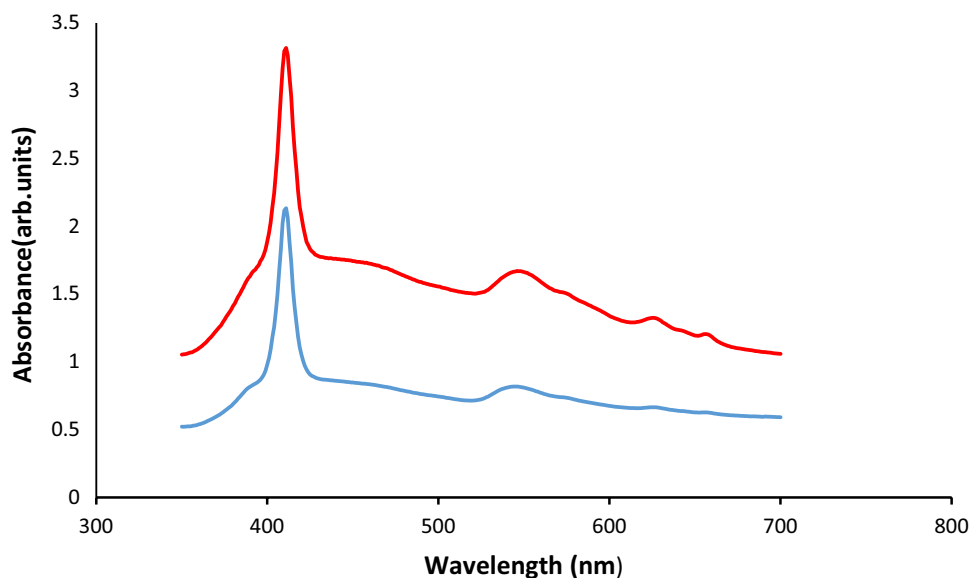
of PdCu particles deposited on TPPCu, with particle sizes of approximately 100 nm, were observed. Nanoclusters of the same material smaller than 25 nm were also dispersed on the surface of the support. This suggests that Cu-coordinated metalloporphyrins are suitable for the deposition of Cu-containing catalysts. Similarly, another coordinated porphyrin can be used to deposit a catalyst with the same chemical coordination element. This can improve the electrocatalytic response of the synthesized materials.

Figure 5 shows the EDAX plot of the chemical contents of Pd and Cu in a sample of the PdCu/TPPCu catalyst. The

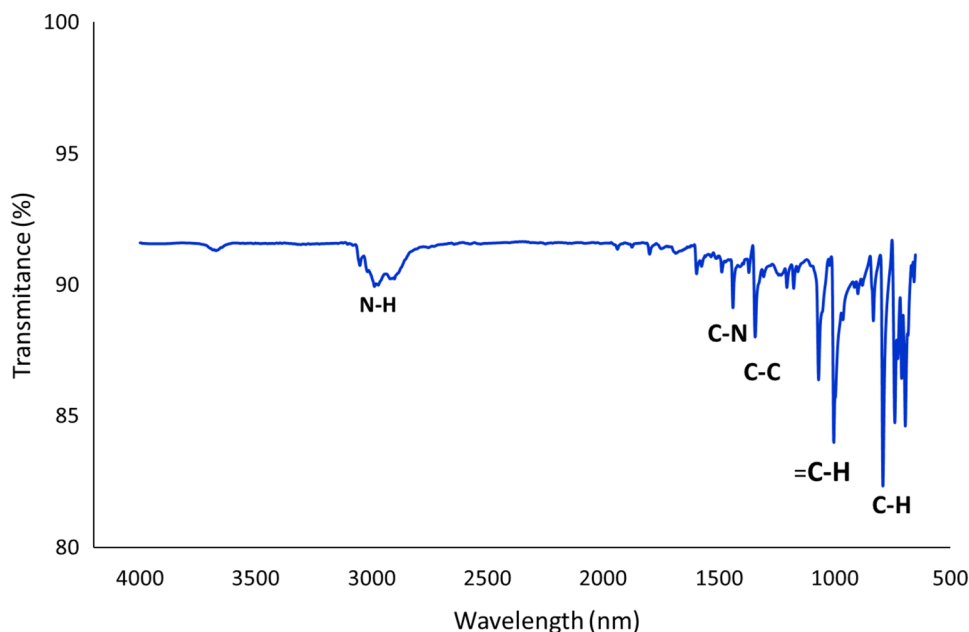
sample contains 56.36% Pd and 43.64% Cu. The chemical composition spectrum and reported values were obtained after subtracting the data corresponding to TPPCu to report a more appropriate value of the catalyst. That is, Cu coordinated to porphyrin was not included. The stoichiometric ratio indicates that the electrocatalyst was slightly enriched in Pd (Cu/Pd=0.77). This probably promotes electrochemical processes while maintaining kinetic properties.

Figure 6 shows the UV–vis/NIR spectrum of Pd-Cu/TPPCu. A Soret peak was observed at 411 nm with an absorbance of 2.01%. The peak at 547 nm, known as the

**Fig. 6** UV–vis/NIR spectrum of Pd-Cu/TPPCu (blue line) and TPPCu (red line)



**Fig. 7** FTIR spectrum of Pd-Cu/TPPCu



Q peak, exhibited an absorbance of 0.81%, indicating that TPPCu had a low absorbance value in this region. This result suggests that TPPCu was not modified by the presence of the synthesized electrocatalyst because of the existence of a stable  $\pi$ -electron conjugated system of metalloporphyrin. The UV–Vis/NIR spectra of metalloporphyrin before and after the electrocatalyst synthesis were similar. This suggests that the metalloporphyrin-conjugated system did not undergo deprotonation because of synthesis effects. This indicated that metalloporphyrin was stable in the reaction medium. However, this characterization technique does not provide information about the physicochemical interactions between the support and electrocatalyst.

The improvement in the catalytic performance of Pd in the presence of TPPCu was attributed to the synergistic effect of the components. There is likely an adequate dispersion of the Pd–Cu electrocatalytic particles on TPPCu, which increases the number of active sites and improves the adsorption and transport of reactants and products on the surface. Finally, the catalytic efficiency of the synthesized material and its tolerance to CO during the electrochemical oxidation of alcohols can be improved. Furthermore, TPPCu could act as a stabilizer during the deposition of Pd on its surface because of the attraction sites related to the metal coordination centers.

Figure 7 shows the FTIR spectrum of PdCu/TPPCu. This characterization confirmed that the presence of the PdCu based electrocatalyst did not affect the composition of TPPCu. Functional groups related to TPPCu were identified at 2972 nm, which corresponded to the N–H functional group. This is mainly associated with the organic part of TPPCu. The broadened shape of this peak indicates that the

TPPCu sample was not deprotonated during the electrocatalytic synthesis. It is also possible to observe a peak at approximately 1441 nm, which is associated with the C–N functional groups and is one of the characteristic peaks of the acetate ion ( $\text{CH}_3\text{COO}^-$ ). As this peak becomes more defined, it promotes the cleavage of ethanol molecules from the C–C bonds. In addition, the peak observed at 1344 nm has been associated with the selectivity of ethanol electro-oxidation [31]. The peak at 1344 nm is also related to C–C bonds, whereas the peaks at 1003 and 789 nm correspond to C–H bonds. These latter chemical bonds could be related to the electro-oxidation of ethanol via the transfer of 12 electrons and  $\text{CO}_2$  as a by-product.

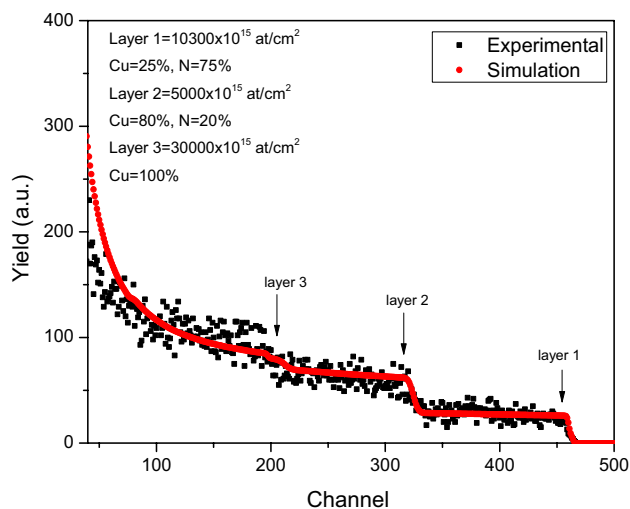


**Fig. 8** RBS spectrum of commercial TPPCu



RBS measurements confirmed the presence of Cu and N in the commercial TPPCu. Figure 8 shows a typical RBS spectrum composed of layers of different thicknesses throughout the material. Layer 1 is located from the surface to 10,300 atomic layers inside the material (1015 at/cm<sup>2</sup> corresponds to 1 atomic layer), while two other layers were detected corresponding to different thicknesses and concentrations of Cu and N throughout the material. As shown in the inset of Fig. 8, the elemental concentration of each layer was different, suggesting that the composition of commercial TPPCu was inhomogeneous. In this material, the Cu concentration increases from 25% at the surface to 100% in layer 3.

Figure 9 shows the RBS spectrum of the PdCu/TPPCu sample. Contrary to what is shown in Fig. 8, the PdCu/TPPCu prepared in our laboratory is a homogeneous material whose main components are 25% Cu and 75% Pd throughout the material. It should be noted that because of the low Rutherford cross-section of C and N, it was not possible to detect these elements, but this does not mean that they were not present in the sample, as they were detected by EDS. The PdCu-based electrocatalyst was exposed on the surface of the electrocatalyst, whereas TPPCu remained under the electrocatalyst and acted as a support. The experimental data for PdCu/TPPCu were compared with the simulation results using the SIMNRA code (red line). The simulation results agreed with the theoretical data, indicating that the synthesized material was a solid phase formed by a catalytic layer supported on an organometallic molecule. The simulation was performed by entering data such as the type of projectile and its energy; the incident, exit, and scattering angles; and the theoretical composition of the material.

The ethanol electro-oxidation reaction was performed for 50 cycles under the conditions described in

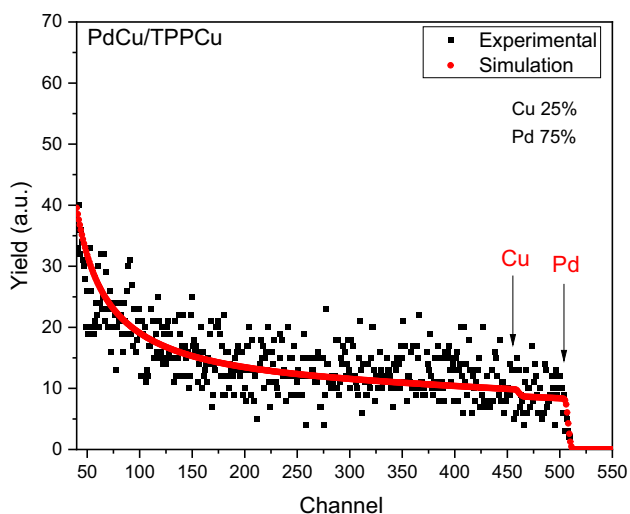


Fig. 9 RBS spectrum of PdCu/TPPCu

the Experimental section. The electrochemical window in which the activation cycle was performed, as well as all cycles related to the electro-oxidation of ethanol, was from  $-0.8$  to  $0.4$  V/SCE, at a scan rate of  $50$  mV/s. The open-circuit potential ( $-0.109$  V/SCE) was measured to ensure the stability of the electrocatalyst in a  $1$  M KOH solution.

Figure 10 shows the voltammograms of electrocatalyst activation (orange line), cycle 1 (green line), and cycle 50 (blue line) of the EOR. The activation voltammogram shows no reaction peaks or degradation signals in the electrocatalyst. In addition, the onset potential started at  $-0.41$  V/SCE in cycle 1. A maximum current ( $j_{\max}$ ) of  $0.02$  mA/cm<sup>2</sup> was found at  $-0.31$  V/SCE (peak (a)). The EOR performed on the electrocatalyst did not exhibit any reoxidation peaks corresponding to the adsorption of CO species. In cycle 50, the EOR starts at  $-0.64$  V/SCE. The  $j_{\max}$  was  $0.20$  mA/cm<sup>2</sup> at  $-0.37$  V/SCE (peak (b)). During the fifty cycles, the formation of an adsorption peak at  $0.05$  V/SCE (peak (c)) was observed, as well as the formation of a reoxidation peak at  $-0.39$  V/SCE with a  $j_{\max}$  of  $0.33$  mA/cm<sup>2</sup> (peak (d)).

The previously obtained results refer to the active surface of PdCu/TPPCu. So, the electrochemical active surface (EAS) was calculated according to Eq. (2).

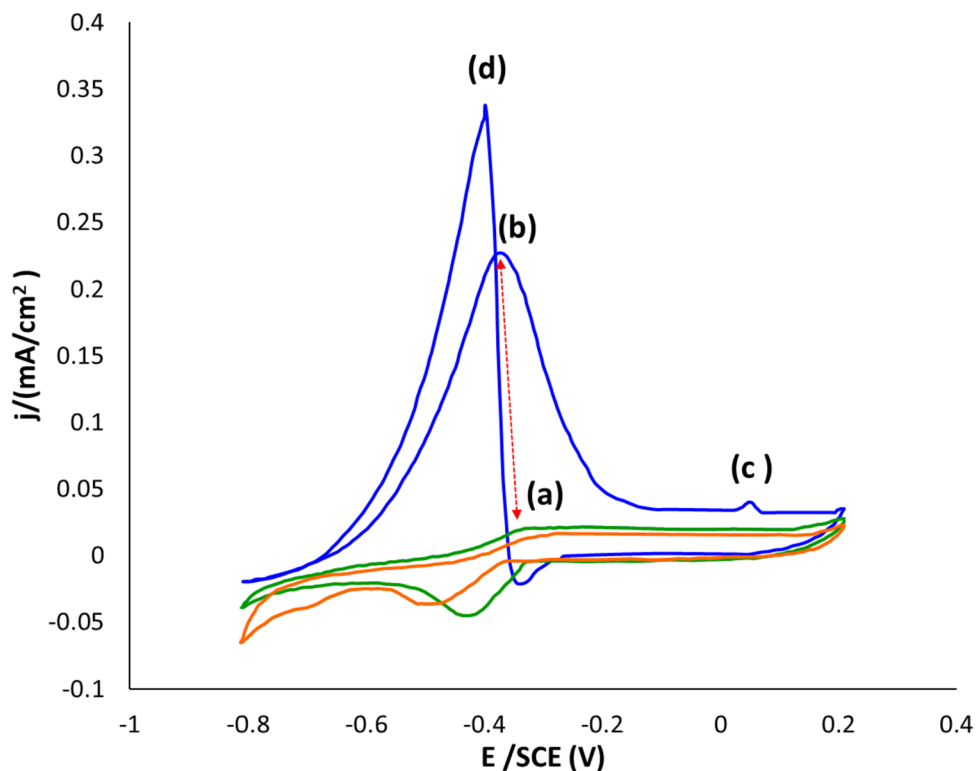
$$EAS = \frac{Q_H}{k \times L} \quad (2)$$

where  $L$  is the mass of the PdCu/TPPCu electrocatalyst on the electrode surface (mg/cm<sup>2</sup>),  $k$  is the charge constant of the electrocatalytic surface ( $44,200$  mC/m<sup>2</sup>), and  $Q_H$  is the hydrogen electroadsorption (mC/cm<sup>2</sup>). The  $Q_H$  of PdCu/TPPCu was  $43,700$  mC/cm<sup>2</sup>. The EAS of PdCu/TPPCu is  $49.4$  m<sup>2</sup>/g. It is  $6.4$  times larger than the area reported for commercial Pd/C [32]. This indicates that the use of TPPCu as a support may be a suitable method to improve the mass transport in Pd-based catalytic systems.

Table 1 summarizes the electrical characteristics of the EOR between cycles one and 50. This result indicates that intermediate species are formed on the electrocatalyst due to EOR, which is typical for Pd-based electrocatalysts. However, the reaction potential remains almost unchanged. This is an indication of the tolerance to CO poisoning.

The results obtained for the electro-oxidation reaction indicated that the electrocatalytic response in cycle 50 was better than that in cycle 1. This suggests that a higher amount of ethanol adsorbed on TPPCu after 50 cycles could increase the number of species susceptible to electro-oxidation during the reaction. It suggests a synergistic effect between PdCu and TPPCu in the anodic reactions. The electro-oxidation reaction onset potential in Cycle 50 is lower than that in Cycle 1,  $-0.64$  and  $-0.41$  V/SCE, respectively. These

**Fig. 10** Cyclic voltammograms on PdCu/TPPCu. A solution of 1 M ethanol and 1 M KOH was used as the electrolyte. The scan rate was 50 mV/s. Activation of the electrocatalyst (orange line). Cycles 1 and 50 (green and blue lines, respectively) correspond to the ethanol oxidation reaction



results can be related to the adequate performance of the electrocatalyst with the support material, which promotes a combined effect between the availability of the adsorbed species and the feasibility of releasing the by-products and species generated during the electro-oxidation reaction.

Table 2 summarizes the onset potential and current density of some Pt- or Pd-based catalysts for the ethanol

**Table 1** Onset potential values and maximum currents in cycles 1 and 50 of the EOR on the PdCu/TPPCu electrocatalyst

Cycles	E (onset potential) (V/SCE)	$j_{\max}$ (mA/cm <sup>2</sup> )
1	-0.41	0.02
50	-0.64	0.20

**Table 2** Comparison between Pt- and Pd-based catalysts for performing the ethanol oxidation reaction in 1 M KOH + 1 M CH<sub>3</sub>CH<sub>2</sub>OH

Catalysts	Electrolyte	E/SCE (V)	$j$ (mA cm <sup>2</sup> )	References
Pd <sub>2</sub> Cu/Ni <sub>2</sub>	1 M	0.375	3.6	[33]
Pt-ZrO <sub>2</sub> /C	KOH + 1 M	-0.25	25	[34]
Pd	CH <sub>3</sub> CH <sub>2</sub> OH	-0.235	5.1	[35]
Pt		-0.276	7.4	
Cycle 1 PdCu/TPPCu		-0.41	0.02	This work
Cycle 50 PdCu/TPPCu		-0.64	0.20	

oxidation reaction. The experiments were performed in an electrolyte consisting of 1 M KOH + 1 M CH<sub>3</sub>CH<sub>2</sub>OH at room temperature. Pt and Pt-ZrO<sub>2</sub>/C showed the highest reaction current densities compared to Pd-based catalysts because of the noble metal nature of Pt. The ZrO<sub>2</sub>/C supported catalyst showed a higher current density than Pt. This was probably due to the better distribution of oxidizable and oxidized species on the support surface. In the case of Pd-based catalysts (Pd<sub>2</sub>Cu/Ni<sub>2</sub> and Pd), the current densities were similar for both materials. This is related to the intrinsic catalytic behavior of Pd in alkaline media. Finally, by comparing the above catalysts with the material synthesized in this work, it can be noted that the onset potential of the ethanol electro-oxidation reaction on PdCu/TPPCu was lower than that obtained for the other catalysts. This catalyst can be used in direct ethanol fuel cells, where lowering the activation energy is still a challenge for anodic catalysts. However, the current density generated on this catalyst was the lowest among all the catalysts. This was probably due to the low catalytic load deposited on the metalloporphyrin, which limited the surface area of the catalyst.

Figure 11 shows voltammograms of the ethanol oxidation reaction at different scan rates. This study was performed in an electrolyte containing 1 M KOH + 1 M CH<sub>3</sub>CH<sub>2</sub>OH. The onset potential varied as a function of the applied scan rate as follows: -0.36, -0.62, and -0.58 V/SCE at 10, 30, and 100 mV/s, respectively. This result indicates that the variation in the reaction thresholds is a function of the catalyst

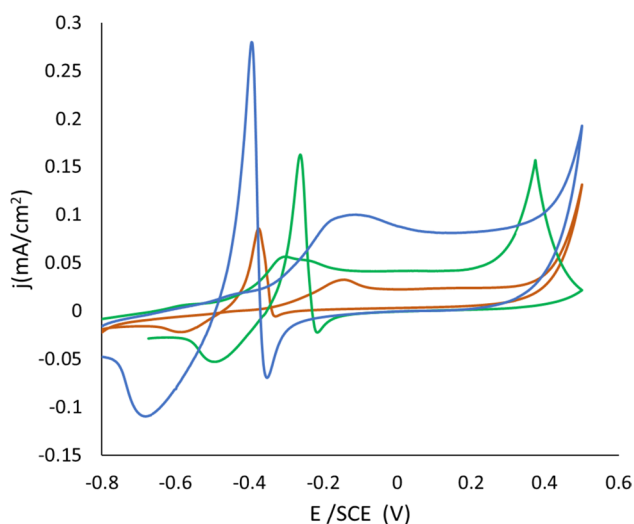


**Fig. 11** Voltammograms of the electro-oxidation of 1 M  $\text{CH}_3\text{CH}_2\text{OH}$  in 1 M KOH. At different scan rates. 10 mV/s (orange line). 30 mV/s (green line). 100 mV/s (blue line)

surface conditions, especially the interaction of the reactants and products on the electronically conductive support. In the case of the reoxidation reaction, changes in the potential threshold are defined by the number of species adsorbed on the surface. In this case, the changes in the onset potentials were smaller than those of the oxidation reaction. Values of  $-0.14$ ,  $-0.3$ , and  $-0.11$  V/SCE were obtained at 10, 30, and 100 mV/s, respectively. It was also observed that at 100 mV/s, the re-oxidation reaction required more energy owing to the charge transition and the transients of the applied potential on the catalyst surface.

Impedance spectroscopy analysis was used to study the kinetic response of the electrode to different ethanol concentrations (1, 2, and 3 mol). The impedance spectra (Fig. 12) were obtained in the range of 1 Hz to 10 kHz, using the open-circuit potential as the reference measurement. In all the cases, the experimental data are shown as blue dots, and the results of the electrical model are shown as solid red lines.

Figure 12a shows the Nyquist plot of PdCu/TPPCu in the absence of ethanol (only 1 M KOH). The response of the catalytic system was dominated by the diffusion effect, which could be mainly related to ions passing from the solution to the synthesized material.

Figure 12b shows the Nyquist response when 1 M  $\text{CH}_3\text{CH}_2\text{OH}$  is added to the system. In this case, there was an impedance change in the high- and mid-frequency regions, indicating the presence of a new electrical process at the electrode. This effect was observed near zero values on the Zreal axis. This result indicates that ethanol is adsorbed by the catalytic surface of the material, which modifies the electrical response of the system. The same process was

observed for the incorporation of 2 mol and 3 mol of ethanol (Fig. 12c and d, respectively). The adsorption of ethanol on the catalytic surface of PdCu/TPPCu was proportional to the alcohol concentration in the medium. However, in all cases, the diffusive component of the electrode was maintained. The ability of the catalytic surface to exchange ions with the solution remained almost constant regardless of the alcohol concentration.

Randles with diffusion ( $R_s + (C_{dl} // (R_{ct} + W))$ ) was used to determine the electrical components. Where  $R_s$  is the solution resistance,  $C_{dl}$  is the double-layer capacitance,  $R_{ct}$  is the charge transfer resistance, and  $W$  is Warburg diffusion. The results shown in Table 3 indicate that the charge transfer resistance changed from 492.5  $\Omega$  when the catalyst was immersed in 1 M KOH to 1800  $\Omega$  when it was immersed in 3 M  $\text{CH}_3\text{CH}_2\text{OH}$ . Intermediate resistance values were obtained for 1 and 2 molar alcohol. Similarly, the exchange current density ( $i_0$ ) (calculated using Eq. (3)) decreased by an order of magnitude as the ethanol concentration increased from 1 to 3 M (0.0129 and 0.007, respectively). This result indicates that the kinetic response to ethanol oxidation is strongly influenced by ethanol concentration in the medium.

$$i_0 = \frac{RT}{nFR_{ct}} \quad (3)$$

where  $R$  is the gas constant (8.314 J/mol·K),  $F$  is the Faraday constant (96,485.33212 J/V·mol),  $n$  is the number of electrons involved in the charge transfer reaction ( $n=2$ ), and  $T$  is the ambient temperature in Kelvin (295 K).

Finally, reagent grade ethanol, agave bioalcohol (heart), and agave bioalcohol residues (distillate tails) were used in an experimental fuel cell with the synthesized material as the anode catalyst. These experiments demonstrated the feasibility of producing sustainable energy using different alcohols as fuels in an electrochemical system.

Figure 13 shows the polarization curves when three different alcohols were introduced into the experimental fuel cell. Figure 13a shows the electrical response of the fuel cell to reagent-grade ethanol. It produced an open circuit potential (OCP) of 0.8 V, which is adequate for an alcohol fuel cell operating at room temperature. In this case, the fuel cell produced a short-circuit current (SCC) of approximately 1.9 mA/cm<sup>2</sup>. The ohmic region of the fuel cell indicates a good mechanical assembly process with electrocatalytic electrodes. Figure 13b shows the electrical power curve of the ethanol fuel cell, which produces a maximum power of 0.4 mW/cm<sup>2</sup> at the maximum current of 1 mA/cm<sup>2</sup>.

Figure 13c shows the electrical characteristics of the fuel cell fed with bioethanol (agave distillate heart). The cell produces an open-circuit voltage of 0.75 V and a short-circuit current of approximately 0.9 mA/cm<sup>2</sup>. The maximum electrical power produced by this fuel cell was 0.16 mW/cm<sup>2</sup>

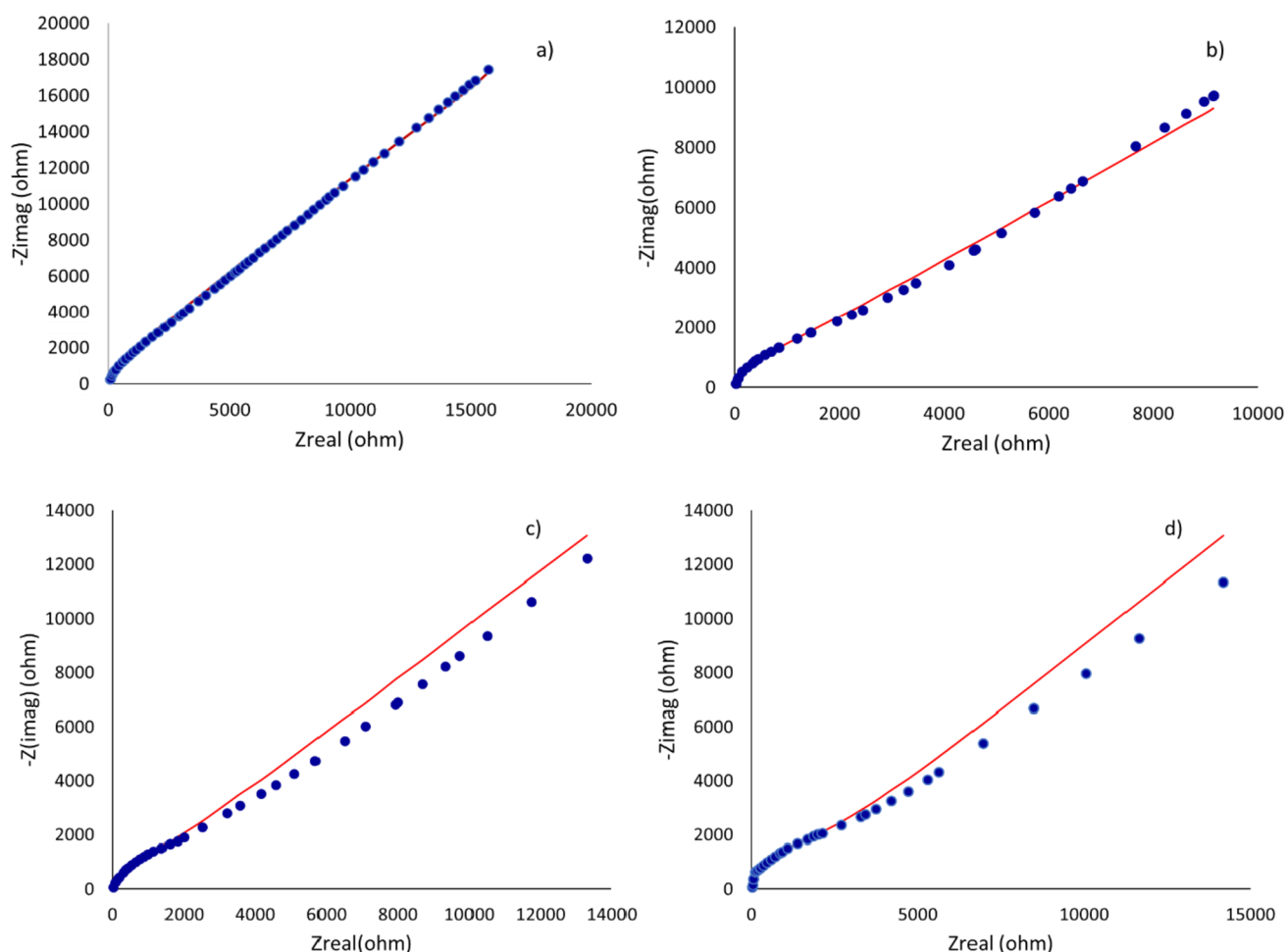


**Fig. 12** Nyquist plots obtained by EIS on PdCuTPPCu. 1 M KOH (a). 1 M KOH + 1 M CH<sub>3</sub>CH<sub>2</sub>OH (b). 1 M KOH + 2 M CH<sub>3</sub>CH<sub>2</sub>OH (c). 1 M KOH + 3 M CH<sub>3</sub>CH<sub>2</sub>OH (d)

at a discharge current of 0.5 mA/cm<sup>2</sup> (Fig. 13d). The cell produced 40% less electrical power when using bioethanol as fuel than when using ethanol.

When the fuel cell was fed with agave distillate tails (waste bioethanol), the electrical response was similar to that when fed with bioethanol. In this case, the open-circuit potential was 0.76 V, the short-circuit current was 0.9 mA/

cm<sup>2</sup> (Fig. 13e), and the maximum electrical power was 0.17 mW/cm<sup>2</sup> at a current of 0.51 mA/cm<sup>2</sup> (Fig. 13f).

Although the difference in the results is minimal, it can be observed that a fuel cell fed with waste bioethanol can produce the same or more electric power than when bioethanol is used. This may be due to the number of short- and long-chain alcohols present in the waste, which can produce sufficient energy when in contact with the selective electrocatalysts. Another possibility is related to the support material used to properly handle the diffusive transport of reactants and products to improve mass and energy transitions through the electrocatalysts. Finally, the combined use of waste bioethanol and supported electrocatalysts on organometallic molecules could be considered for the development of new sustainable energy production systems.

**Table 3** Kinetic values obtained by EIS for different molar concentrations

Concentration	R <sub>s</sub> (Ω)	C <sub>dl</sub> (F) x10 <sup>-6</sup>	R <sub>ct</sub> (Ω)	W1 (S*s <sup>1/2</sup> ) x10 <sup>-6</sup>	i <sub>0</sub> (mA)
1 M KOH	16.73	2.89	492.5	3.79	0.0258
1 M ethanol	16.46	2.25	978	4.71	0.0129
2 M ethanol	17.57	2.26	1107	5.51	0.0114
3 M ethanol	18.26	2.38	1800	5.94	0.0070

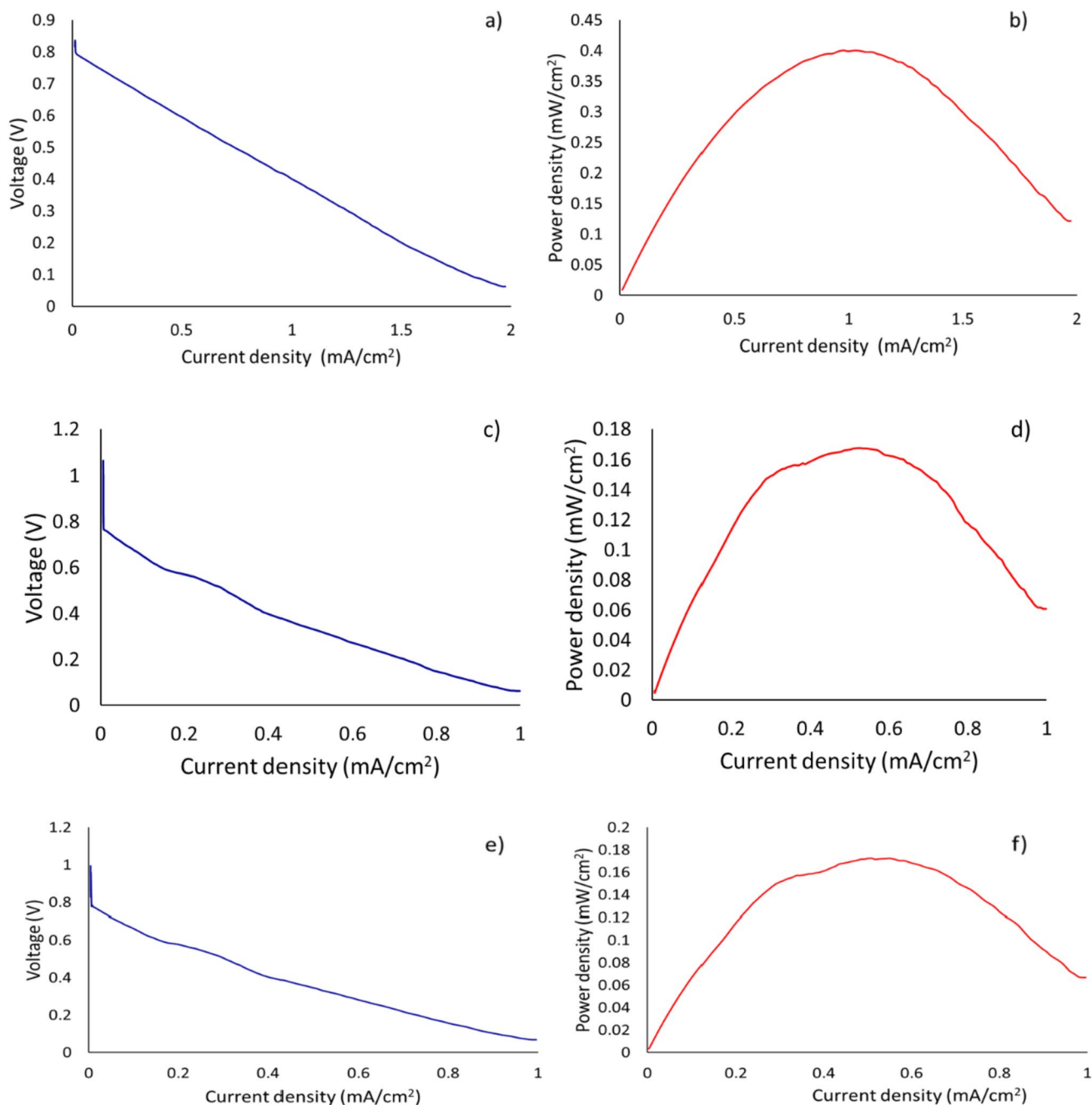


**Fig. 13** Polarization curves of fuel cells fed reagent grade ethanol (a)–(b), bioalcohol (hearts) (c)–(d), and bioalcohol residue (tails) (e)–(f). The catalytic loading on the anodic side was 8 mg of PdCu/TPPCu diluted in 25  $\mu$ L of liquid Nafion and 50  $\mu$ L of  $C_3H_8O$ . On

the cathodic side, 8 mg of commercial Pt/C diluted in 25  $\mu$ L of liquid Nafion and 50  $\mu$ L of  $C_3H_8O$  were deposited. In each experiment, 5  $\mu$ L of alcohol was used at the anode, and air at atmospheric pressure was used at the cathode

## 4 Conclusions

TPPCu was investigated as a support for the Pd–Cu electrocatalyst in ethanol fuel cell applications. The synthesis of Pd–Cu on TPPCu prevented metalloporphyrin deprotonation and enabled the electro-oxidation of ethanol with

tolerance to CO poisoning. TPPCu as an electrocatalytic support may allow mass and energy transport on the Pd–Cu surface to enhance the ethanol electro-oxidation reaction during cycling. Evaluation of the supported electrocatalyst in an experimental fuel cell demonstrated the functionality of the material in generating electric power

from the supply of reagent grade ethanol or bioethanol residues. These results suggest that the use of organometallic molecules, such as metalloporphyrins, could improve the electrocatalytic performance and CO poisoning tolerance of current electrocatalysts widely used in alkaline alcohol fuel cells.

**Acknowledgements** The authors thank Ms. Ma. Luisa Ramon-Garcia and Dr. Patricia E. Altuzar-Coello of the Instituto de Energías Renovables-UNAM for the XRD results and structural interpretations. The authors also thank Mr. Gildardo Casarrubias-Segura of the Instituto de Energías Renovables-UNAM for providing the SEM images. Thanks to Mr. Lázaro Huerta-Arcos of the Instituto de Investigaciones en Materiales, UNAM, and Dr. David Avellaneda of the Universidad Autónoma de Nuevo León for the XPS analysis of the samples. Thanks to Dr. Samuel Tehuacanero-Cuapa of the Instituto de Física, UNAM for the TEM and HRTEM analysis of the samples. The authors also thank DGAPA PAPIIT for the grant PAPIIT IN-101122 for support in the synthesis and characterization of materials. Special thanks to CONAH-CYT, Estancias Posdoctorales por México 2022 for the fellowship to Dr. Claudia Karina Zagal-Padilla (464307), and Dr. Shirley Irazoque-Castañeda (425524).

**Author contributions** SIC Data curation, methodology, formal analysis, writing-original draft. Writing responses to reviewers. ALS Data curation, methodology, formal analysis, conceptualization. Writing responses to reviewers and corrected article. CKZP Formal analysis, conceptualization, resources. Writing responses to reviewers and corrected article. SAGS Conceptualization, supervision, funding acquisition, writing-review and editing original draft. Writing responses to reviewers and corrected article, Supervision of revised manuscript. All authors discussed the results and contributed to the final manuscript.

**Funding** This work was supported by DGAPA PAPIIT IN-101122 project.

**Data availability** The complete data are available upon request from the corresponding author.

## Declarations

**Conflict of interest** The authors declare that they have no conflict of interest.

**Open Access** This article is licensed under a Creative Commons Attribution 4.0 International License, which permits use, sharing, adaptation, distribution and reproduction in any medium or format, as long as you give appropriate credit to the original author(s) and the source, provide a link to the Creative Commons licence, and indicate if changes were made. The images or other third party material in this article are included in the article's Creative Commons licence, unless indicated otherwise in a credit line to the material. If material is not included in the article's Creative Commons licence and your intended use is not permitted by statutory regulation or exceeds the permitted use, you will need to obtain permission directly from the copyright holder. To view a copy of this licence, visit <http://creativecommons.org/licenses/by/4.0/>.

## References

- Wang X, Zhu J, Han M (2023) Industrial development status and prospects of the marine fuel cell: a review. *J Mar Sci Eng.* <https://doi.org/10.3390/jmse11020238>
- Miličević Z, Bojković Z (2023) Military green technology: present and future. *Vojnotehnicki glasnik* 71:136–152. <https://doi.org/10.5937/vojtehg71-40544>
- Elsaid K, Abdelfatah S, Abdel Elabsir AM et al (2021) Direct alcohol fuel cells: assessment of the fuel's safety and health aspects. *Int J Hydrogen Energy* 46:30658–30668. <https://doi.org/10.1016/j.ijhydene.2020.12.009>
- Li C, Wang K, Xie D (2022) A review of approaches for the design of high-performance electrocatalysts for ethanol electrooxidation. *Surf Interf* 28:101594. <https://doi.org/10.1016/j.surfin.2021.101594>
- Shaari N, Kamarudin SK, Bahru R et al (2021) Progress and challenges: review for direct liquid fuel cell. *Int J Energy Res* 45:6644–6688. <https://doi.org/10.1002/er.6353>
- Nassif N, Ghayad I, Hamid ZA (2021) Review article: direct ethanol fuel cells as a renewable source of energy. *Egypt J Chem* 64:2723–2729. <https://doi.org/10.21608/EJCHEM.2021.58244.3254>
- Cui Z, Hu J, Jiang X et al (2021) Asymmetric Au/(PdAg alloy) nano-allium giganteums for their enhanced electrocatalytic performances to ethanol oxidation reaction. *J Alloys Compd* 855:157385. <https://doi.org/10.1016/j.jallcom.2020.157385>
- Serrano-Jiménez J, de la Osa AR, Rodríguez-Gómez A et al (2023) Electro-reforming of bioethanol produced by sugar fermentation on a Pt–Ni anodic catalyst supported on graphene nanoplatelets. *J Environ Chem Eng.* <https://doi.org/10.1016/j.jece.2023.109703>
- Ye N, Zhao P, Qi X et al (2022) Ethanol electro-oxidation on the PdSn-TaN/C catalyst in alkaline media: making TaN capable of splitting C[sbnd]C bond. *Appl Catal B.* <https://doi.org/10.1016/j.apcatb.2022.121473>
- Huang X, Yang G, Li S et al (2022) Noble-metal-based high-entropy-alloy nanoparticles for electrocatalysis. *J Energy Chem* 68:721–751. <https://doi.org/10.1016/j.jechem.2021.12.026>
- Singh BK, Mahapatra SS (2023) Performance study of palladium modified platinum anode in direct ethanol fuel cells: a green power source. *J Indian Chem Soc* 100:100876. <https://doi.org/10.1016/j.jics.2022.100876>
- Xu B, Zhang Y, Li L et al (2022) Recent progress in low-dimensional palladium-based nanostructures for electrocatalysis and beyond. *Coord Chem Rev* 459:214388. <https://doi.org/10.1016/j.ccr.2021.214388>
- Wei M, Chen L, Wang X et al (2023) Tubular palladium-based catalysts enhancing direct ethanol electrooxidation. *J Coll Interf Sci* 633:932–947. <https://doi.org/10.1016/j.jcis.2022.11.154>
- Petriev I, Pushankina P, Glazkova Y, Andreev G, Baryshev M (2023) Investigation of the dependence of electrocatalytic activity of copper and palladium nanoparticles on morphology and shape formation. *Coating* 13:2–16. <https://doi.org/10.3390/coatings13030621>
- Liu B, Wu C, Wen C et al (2022) Promoting effect of (Co, Ni)O solid solution on Pd catalysts for ethylene glycol electrooxidation in alkaline solution. *Electrochim Acta* 408:139965. <https://doi.org/10.1016/j.electacta.2022.139965>
- Lao X, Sun T, Zhang X et al (2022) Controllable lattice expansion of monodisperse face-centered cubic Pd–Ag nanoparticles for C1 and C2 alcohol oxidation: the role of core-sheath lattice mismatch. *ACS Sustain Chem Eng.* <https://doi.org/10.1021/acssuschemeng.2c01592>
- Mojabi S, Sanjabi S (2022) Decorated fractal Ni–Cu foam with Pd nanoparticles as a high-performance electrocatalyst toward hydrogen evolution reaction. *Thin Solid Films* 758:139415. <https://doi.org/10.1016/j.tsf.2022.139415>
- Hang H, Altarawneh RM, Brueckner TM, Pickup PG (2020) Pt/Ru–Sn oxide/carbon catalysts for ethanol oxidation. *J Electrochem Soc* 167:054518. <https://doi.org/10.1149/1945-7111/ab7f9e>

19. Wang S, Xu B, Huo W et al (2022) Efficient FeCoNiCuPd thin-film electrocatalyst for alkaline oxygen and hydrogen evolution reactions. *Appl Catal B* 313:121472. <https://doi.org/10.1016/j.apcatb.2022.121472>
20. Hefnawy MA, Medany SS, El-Sherif RM et al (2023) High-performance IN738 superalloy derived from turbine blade waste for efficient ethanol, ethylene glycol, and urea electrooxidation. *J Appl Electrochem* 53:1337–1348. <https://doi.org/10.1007/s10800-023-01862-7>
21. Zhou S, Yan R, Zhou W et al (2023) Highly efficient electrooxidation of ethanol on CuPtPd trimetallic catalyst. *J Electroanal Chem* 929:117118. <https://doi.org/10.1016/j.jelechem.2022.117118>
22. Fan Z, Zhang W, Li L et al (2022) Recent developments in electrode materials for the selective upgrade of biomass-derived platform molecules into high-value-added chemicals and fuels. *Green Chem* 24:7818–7868. <https://doi.org/10.1039/d2gc02956a>
23. Torres P, Guillén M, Escribà M et al (2023) Synthesis of new amino-functionalized porphyrins: preliminary study of their organophotocatalytic activity. *Molecules*. <https://doi.org/10.3390/molecules28041997>
24. Dong Y, Nie R, Wang J et al (2019) Photoelectrocatalytic CO<sub>2</sub> reduction based on metalloporphyrin-modified TiO<sub>2</sub> photocathode. *Chin J Catal* 40:1222–1230. [https://doi.org/10.1016/S1872-2067\(19\)63375-9](https://doi.org/10.1016/S1872-2067(19)63375-9)
25. Nishiori D, Wadsworth BL, Reyes Cruz EA et al (2022) Photoelectrochemistry of metalloporphyrin-modified GaP semiconductors. *Photosynth Res* 151:195–204. <https://doi.org/10.1007/s11120-021-00834-2>
26. Xia Y, Shuai L, Wang Y et al (2020) Designing bifunctional molecular devices with a metalloporphyrin dimer. *Phys Chem Chem Phys* 22:4080–4085. <https://doi.org/10.1039/c9cp05079e>
27. Wu JB, Lin YF, Wang J et al (2003) Correlation between N 1s XPS binding energy and bond distance in metal amido, imido, and nitrido complexes. *Inorg Chem* 42:4516–4518. <https://doi.org/10.1021/ic034261w>
28. Kim A, Muthuchamy N, Yoon C et al (2018) MOF-derived Cu@Cu<sub>2</sub>O nanocatalyst for oxygen reduction reaction and cycloaddition reaction. *Nanomaterials* 8:1–13. <https://doi.org/10.3390/nano8030138>
29. Saphier M, Yifrah T, Zilbermann I et al (2012) The redox chemistry of copper tetraphenylporphyrin revisited. *J Porphyr Phthalocyan* 16:1124–1131. <https://doi.org/10.1142/S108842461250112X>
30. Liu J, Zhang Z, Li Y et al (2023) An ultrasensitive electrochemical immunosensor for carcinoembryonic antigen detection based on two-dimensional PtPd/Cu-TCPP(Fe) nanocomposites. *Anal Bioanal Chem* 415:447–456. <https://doi.org/10.1007/s00216-022-04425-5>
31. Qin Y, Wang F, Liu P et al (2023) Enhancement of CH<sub>3</sub>CO\* adsorption by editing d-orbital states of Pd to boost C-C bond cleavage of ethanol electrooxidation. *Sci China Chem* 66:1–9. <https://doi.org/10.1007/s11426-023-1756-8>
32. Xu H, Yan B, Zhang K et al (2018) Sub-5nm monodispersed PdCu nanosphere with enhanced catalytic activity towards ethylene glycol electrooxidation. *Electrochim Acta* 261:521–529. <https://doi.org/10.1016/j.electacta.2018.01.004>
33. Bai Y, Gong X, Ye N et al (2022) Design the PdCu/Ni<sub>2</sub>P electrocatalyst with high efficiency for ethanol oxidation reaction in alkaline media. *Int J Hydrogen Energy* 47:1543–1555. <https://doi.org/10.1016/j.ijhydene.2021.10.016>
34. Bai Y, Wu J, Xi J et al (2005) Electrochemical oxidation of ethanol on Pt-ZrO<sub>2</sub>/C catalyst. *Electrochim Commun* 7:1087–1090. <https://doi.org/10.1016/j.elecom.2005.08.002>
35. Xie SW, Chen S, Liu ZQ, Xu CW (2011) Comparison of alcohol electrooxidation on Pt and Pd electrodes in alkaline medium. *Int J Electrochem Sci* 6:882–888. [https://doi.org/10.1016/s1452-3981\(23\)15042-5](https://doi.org/10.1016/s1452-3981(23)15042-5)

**Publisher's Note** Springer Nature remains neutral with regard to jurisdictional claims in published maps and institutional affiliations.

## Authors and Affiliations

S. Irazoque<sup>1,2</sup> · A. López-Suárez<sup>3</sup> · C. K. Zagal-Padilla<sup>1,2</sup> · S. A. Gamboa<sup>1</sup>

✉ S. A. Gamboa  
sags@ier.unam.mx

<sup>1</sup> Instituto de Energías Renovables, Universidad Nacional Autónoma de México, Privada Xochicalco S/N, Centro, 62580 Temixco, Morelos, Mexico

<sup>2</sup> Centro de Investigación en Ingeniería y Ciencias Aplicadas, Universidad Autónoma del Estado de Morelos,

Av. Universidad 1001, Edificio 48, Col. Chamilpa, 62209 Cuernavaca, Morelos, Mexico

<sup>3</sup> Instituto de Física, Universidad Nacional Autónoma de México, A.P. 20-364, 01000 Mexico City, Mexico